02,10

Superconductivity of the In−Ag alloy embedded into a porous glass

© M.V. Likholetova[1], E.V. Charnaya[1,¶], P.D. Lozanskaya[1], Yu.A. Kumzerov[2], A.V. Fokin[2]

[1] St. Petersburg State University,
St. Petersburg, Russia
[2] Ioffe Institute,
St. Petersburg, Russia

¶ E-mail: e.charnaya@spbu.ru

Received October 30, 2025
Revised October 30, 2025
Accepted November 1, 2025

Studies of superconductivity in the porous glass/eutectic In−Ag alloy nanocomposite were carried out. We measured temperature dependences of magnetization at different magnetic fields under the ZFC, FCC, and FCW protocols, as well as the magnetization isotherms. Two superconducting transitions with remarkably different changes of their temperatures with changing magnetic field were found. The magnetic field-temperature phase diagram was obtained. Complicated shapes of the magnetization isotherms were revealed. Unusual shifts of the branches of the magnetization isotherms were observed at increasing and decreasing magnetic field. The obtained results were treated assuming the coexistence of strongly and weakly linked indium segregates within the pore network and the emergence of ferromagnetic order at the interface between indium and $AgIn_2$ intermetallic segregates.

Keywords: superconductivity, porous glass/In−Ag alloy nanocomposite, magnetization.

DOI: 10.61011/PSS.2025.10.62626.306-25

1. Introduction

Today, there is a rising interest in the study of nanostructured metallic superconducting alloys, which find ever-widening applications in microelectronics, robotics, and information processing devices [1–3]. The largest focus is on the alloy of indium and gallium, as well as the triple alloy of indium, gallium and tin, which are being considered for the development of superconducting nanoelectronic elements, in particular, self-healing contacts [4,5]. Thin films of In−Ag alloy and layered structures containing this alloy, along with a bulk alloy of indium and silver, are promising materials for low-temperature superconductor connections and stacking, for use in multilayer chip technology and semiconductor wafer bonding [6–8]. Superconductivity has been studied earlier in the quenched films of In−Ag and multilayer structures [9,10].

One of the options for obtaining nanostructured metal alloys is to introduce them into nanoporous matrices such as synthetic opals, porous aluminum oxide or porous glasses. The morphology of such nanocomposites is determined by the geometry of the pore network and the connectivity of particles in the pores with each other. It has been shown that nanoconfinement significantly affects the superconducting properties of metals and alloys. In most cases, nanocomposites based on porous matrices with metals and alloys in the pores exhibit type-II superconductivity with large upper critical fields, the magnitude of which depends on the pore size [11,12]. The change in the type of superconductivity for pure metals is explained by a reduction in the electron free path under nanocontainment conditions. Yet, in case of opal, the pores of which were filled with tin, the conductivity of type-I was reported [13]. Superconductivity in a nanocomposite based on porous glass with an alloy of indium and silver, the composition of which was close to eutectic, was studied in [14]. The magnetic properties of the nanocomposite indicated the coexistence of type-I and type-II supeconductivity. Two transitions to the superconducting state with temperatures of 4.05 and 3.38 K were observed. Shifts in the curves of secondary and tertiary magnetization based on the dependences of magnetization on the applied magnetic field were also revealed, which were interpreted as a result of the emerging of a ferromagnetic order in the alloy under nanoconfinement conditions.

This paper presents the results of a further study of the magnetic properties of a nanocomposite with In−Ag alloy, whose composition was close to the eutectic point, based on porous glass with an average pore size of 13 nm.

2. Sample and experiment

The porous glass used for filling with In−Ag alloy was obtained by heat treatment and leaching of sodium borosilicate glass [15]. The pore size and porosity were determined by nitrogen porosity measurement using a Quadrasorb SI analyzer. The average diameter of pores was equal 13 nm and the volume was about 21 % from the total volume of glass matrix.

The ratio of the components in In−Ag alloy was close to the eutectic point and was 95 at.% In and 5 at.% Ag. The melt was embedded into the pores of the glass matrix under

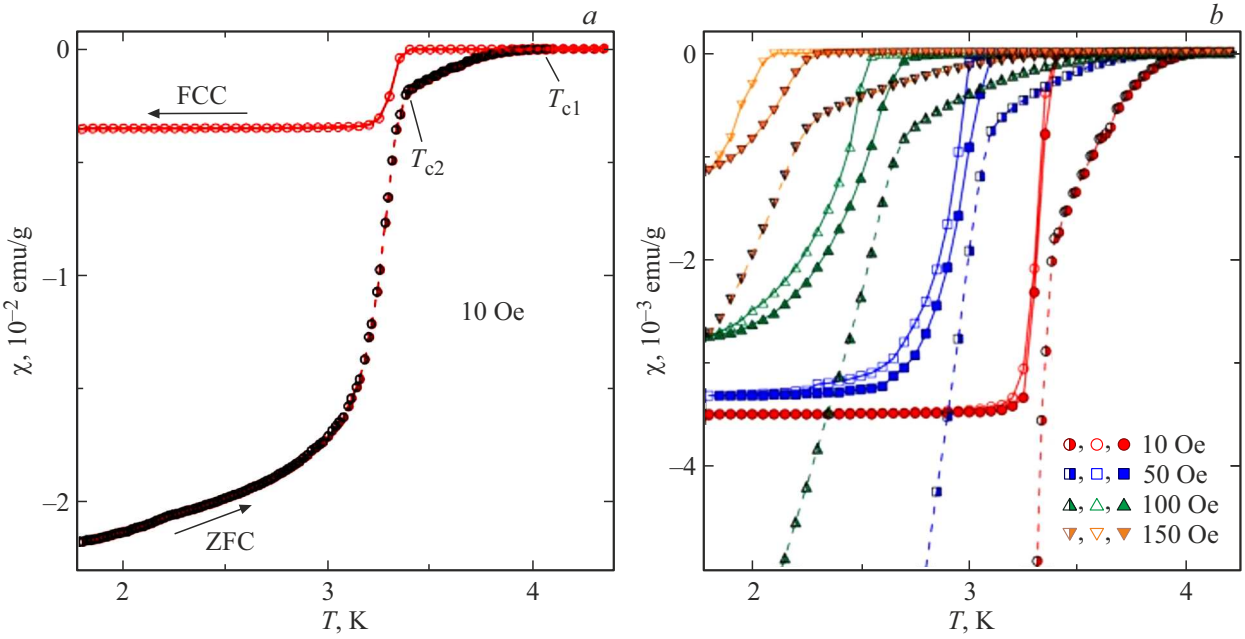

Figure 1. (*a*) Temperature dependences of the susceptibility obtained under ZFC and FCC protocols in 10 Oe field. (*b*) Temperature dependences of the susceptibility obtained under ZFC (half-filled characters), FCC (unfilled characters) and FCW (filled characters) protocols in fields of 10 Oe (circles), 50 Oe (squares), 100 Oe (triangles) and 150 Oe (inverted triangles).

pressure up to 20 kbar. The solidus temperature for In–Ag bulk alloy with a high indium composition is 417 K [16–18]. Below the solidus line, the alloy consists of indium and $AgIn_2$ intermetallic segregates. The measurement sample was cut from an alloy-filled porous glass in the form of a plate. The surface of the sample was thoroughly cleaned from traces of bulk alloy. The sample mass was 7.37 mg.

Static magnetization (dc magnetization) M versus temperature and magnetic field was measured using a Quantum Design MPMS3 SQUID-VSM magnetometer within the temperature range 1.8 to 10 K at applied magnetic fields up to 70 kOe. Measurements at different temperatures were carried out at warming in the field of up to 10 K after the sample had been cooled from the room temperature down to 1.8 K in a zero magnetic field (zero-field cooled — ZFC) followed by cooling down to the minimal temperature (field-cooling cooling — FCC) and further warming (field-cooling warming — FCW). The magnetization isotherms were measured after cooling the sample from room temperature in a zero field while cycling the field in the range from −70 to 70 kOe at a constant temperature. During the measurements, the surface of the plate was oriented parallel to the applied field.

3. Results and discussion

The temperature dependences of the specific susceptibility calculated from magnetization curves in 10 Oe field obtained at the first warming (ZFC) and subsequent cooling (FCC) are shown in Figure 1, *a*. Two superconducting transitions with temperatures $T_{c1} = 4.05$ K and $T_{c2} = 3.38$ K are visible, which were defined as the beginning of a noticeable deviation of ZFC susceptibility curve from the behavior at higher temperatures. In the temperature range between the first and second transitions, partial shielding of the external field is observed, which shows that the superconducting currents cover only a part of the sample. A huge difference between ZFC- and FCC-susceptibility in this temperature range is an evidence of the onset of type-II superconductivity and a strong pinning of the superconducting vortices. Below the second superconducting transition, the difference between the ZFC and FCC susceptibilities is significantly reduced. Estimation of the volume ZFC-susceptibility calculated from the data in Figure 1, *a*, is close to $-1/4\pi$, which corresponds to the shielding of the entire sample volume from the magnetic field by superconducting currents. In Figure 1, *b* the sensitivity curves obtained by applying several magnetic fields in all three measurement modes are shown on an enlarged scale. Figure 1, *b* demonstrates the temperature shift of both transitions to the superconducting state as the applied magnetic field increases. It can be seen that the transition at a higher temperature shifts significantly weaker with increasing field than the second transition, which is not observed in fields above 150 Oe. Note that the FCC and FCW curves are different in limited temperature ranges below the second superconducting transition.

The temperature of the second transition $T_{c2} = 3.38$ K in 10 Oe field is very close to the temperature of the superconducting transition in zero field in the bulk crystal of indium, equal to 3.414 K. This suggests that the second transition is a transition to the superconducting state of

indium segregates. The strong diamagnetic shielding at low temperature, seen in Figure 1, corresponds to a high concentration of indium in the alloy. The nature of the first superconducting transition allows for various interpretations. Since superconductivity has not been detected in bulk intermetallic $AgIn_2$, and theoretical calculations predict that the temperature of the superconducting transition in it should not exceed 3 K [19], the first transition is not associated with the $AgIn_2$ segregates. The appearance of superconductivity was observed for amorphous indium at about 4 K [20] with a high critical field of 23 kOe at zero temperature. Thus, the first transition can be explained by the existence of a small amount of amorphous indium in the matrix pores. However, the formation of small indium segregations in the pores, which are weakly connected with the rest of indium, seems to be the most likely. Nanoconfinement can lead to a significant increase in the temperature of the superconducting transition and an increase in critical fields, as reported in [12,21,22].

Based on the data obtained from the temperature dependences of susceptibility, a phase diagram was constructed demonstrating a decrease in the critical temperature for both superconducting transitions with an increase in the magnetic field (Figure 2). The curvature of the critical line for the second transition is negative, as can be seen in the insert in Figure 2. The negative curvature is consistent with the two-fluid model [23], which predicts the following expression for the critical line:

$$H_c(T) = H_{c0}\left(1 - \frac{T^2}{T_{c2}^2}\right), \qquad (1)$$

where H_{c0} — critical field at zero temperature. Approximation of experimental data for the second transition by formula (1) gives the value $H_{c0} = 270$ Oe, close to the value of the critical field for bulk indium 285.7 Oe [24].

The phase diagram in Figure 2 shows that the superconductivity below the first phase transition does not collapse even in 15 kOe field. At higher fields, the first transition shifts below 1.8 K. The large values of the critical fields indicate that the superconductivity below the first transition belongs to type-II superconductivity. The critical line in the phase diagram for the first phase transition has a positive curvature for magnetic fields below 5 kOe. At high fields, the curvature of the critical line becomes negative. A positive curvature of the critical line has been observed for many high-temperature superconductors, as well as for nanostructured type-II superconductors (see [25–27] and references). In case of nanocomposites based on dielectric porous matrices with metallic superconductors embedded in the pores and having a dendritic interface surface, the positive curvature can be interpreted based on the model proposed in [28]. In this study, the structure of alternating layers in the superconducting and normal state is considered, and the proximity effect is taken into account. The fitting curve for the first superconducting transition, obtained by formula (13) from Reference [28], is shown in Figure 2 with a dashed line.

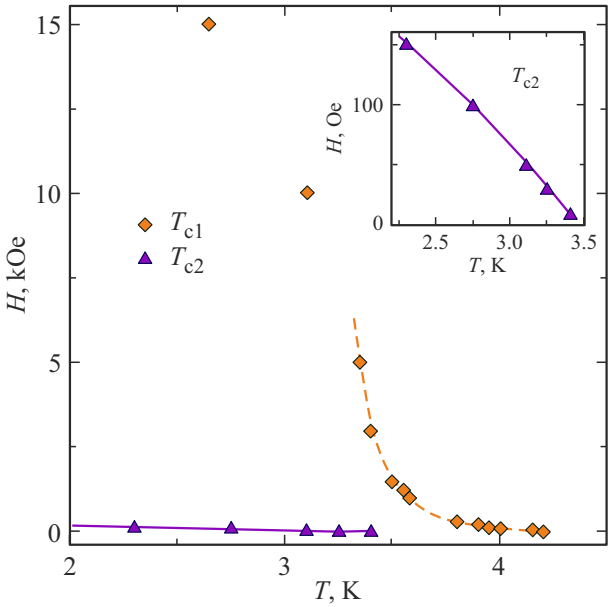

Figure 2. Field-temperature phase diagram. Diamonds and triangles — data for the first and second superconducting transitions, respectively. The insert shows the phase diagram for the second transition on an enlarged scale. The solid line in the figure and inset — an approximation using the formula (1). Dashed line — an approximation using the formula (13) from [28].

The upper insert in Figure 3 shows the $M(H)$ isotherm obtained at $T = 2.3$ K. On an enlarged scale, this isotherm is shown in Figure 3. It can be seen that the hysteresis loop is an overlap of two loops with a larger and a smaller critical field. The existence of two separate hysteresis loops is supported, in particular, by the magnetization isotherm obtained by cycling the field in the range from −200 to 200 Oe, which is shown in the lower insert in Figure 3. The central part of this isotherm did not change, since the cycling limits exceeded the corresponding value of the critical field at this temperature. The magnetization isotherms obtained at other temperatures are given in [14]. The hysteresis loop in Figure 3 with a low critical field correspond to indium segregates with a superconducting temperature of T_{c2}. This loop is partially reversible, which is consistent with the weak pinning in Figure 1. The critical field for segregates with a superconducting temperature T_{c2} is approximately 150 Oe at 2.3 K. This value is close to the critical field equal 147.6 Oe for bulk indium at the same temperature [24]. The shape of the hysteresis loop, characterized by a weak critical field, is typical for real type-I superconductors, as shown by a detailed analysis conducted in [29]. Due to closeness of the temperature T_{c2} to the temperature of the superconducting transition in bulk indium, the coincidence of critical fields in the phase diagram of Figure 2 and the central isotherm in Figure 3 with similar values for bulk indium, the shape of the central hysteresis loop and the weak pinning below the second transition allow us to conclude that the majority of indium

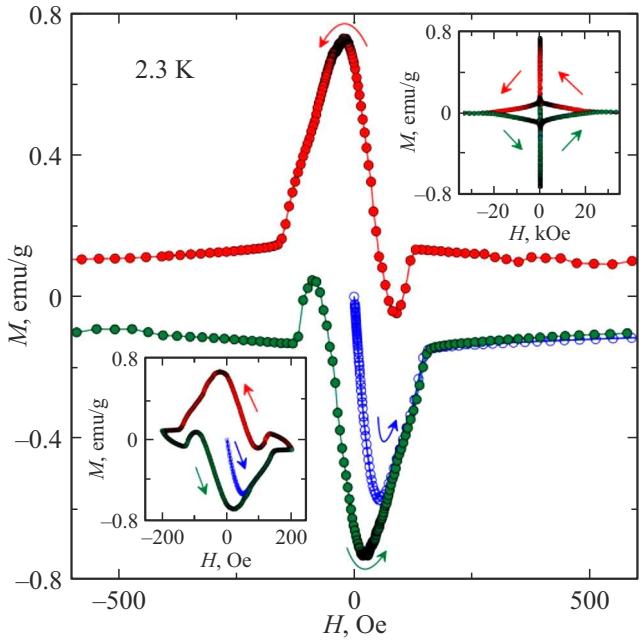

Figure 3. Magnetization isotherm at 2.3 K on an enlarged scale. The upper insert shows the complete hysteresis loop. The lower insert shows the magnetization isotherm measured in the field range from −200 to 200 Oe.

segregates remain type-I superconductors. This conclusion is inconsistent with the results obtained, for example, in [22], where a significantly large critical field and strong pinning indicated the presence of type-II superconductivity for the porous glass-indium nanocomposite. It can be assumed that the type-I superconductivity in indium segregates in the studied nanocomposite in this work is preserved due to better connectivity of indium network because of higher degree of pore filling. In this case, the mean free path of electrons under nanoconfinement does not decrease noticeably and, accordingly, the coherence length remains close to the coherence length in bulk indium.

A special feature of the central part of the hysteresis loop shown in Figure 3, is the shift of the secondary branch of magnetization relative to the primary and tertiary branches. The shift effect has not been observed previously in In–Ag bulk alloy of the same composition. In [14], it was suggested that the relative shift of the magnetization branches is caused by the coexistence of superconductivity and ferromagnetic order at the nanoscale. The nature of this phenomenon is similar to shifts in critical current maxima observed during magnetic field cycling in heterostructures with alternating superconducting and ferromagnetic layers [30–32]. The theoretical interpretation of the anomalous behavior of the critical current is given in the studies [30,33,34]. The sign of the shift of both the magnetization branches and the critical current maxima is determined by the dominant proximity effect. The shift of the branch of secondary magnetization towards negative fields, observed in the present work and in [14], indicates the dominance of residual magnetization effect in ferromagnetic regions (see [32] and references therein). The phenomenon of ferromagnetism in the nanostructured In–Ag alloy requires further study. Bulk $AgIn_2$ intermetallic, like indium, is not magnetic itself. However, it is known that the ferromagnetic order can be established in a number of metals with a decrease in size due to the appearance of uncompensated spins in near-surface regions (see [35,36] and references therein). Following these works and [14], an occurrence of ferromagnetic order at the interface of indium and $AgIn_2$ segregates may be suggested.

The discovered shift of the magnetization branches in In–Ag alloy under nanoconfinement can be compared with studies of magnetization isotherms in porous glass, in which nickel was first chemically introduced, and then the remaining volume inside the pores was filled with indium under pressure. The magnetization isotherm for this nanocomposite, obtained at a temperature of 1.8 K, is shown in Figure 4. Despite the fact that nickel exhibits ferromagnetism within pores, the branches of magnetization do not shift relative to each other. It is possible that the absence of a noticeable shift is explained by the smaller interface area between indium and nickel in the pores.

Figure 1, *b* demonstrates the temperature hysteresis between the FCC and FCW curves. Such hysteresis has been observed in some cases for type-II superconductors, including Ga–Sn alloy in the pores of synthetic opal (see [25] and references therein). The theoretical consideration of hysteresis is based on the assumption that the magnetic flux freezes during cooling [37]. Since most of indium segregates are below the second transition in an intermediate state, as

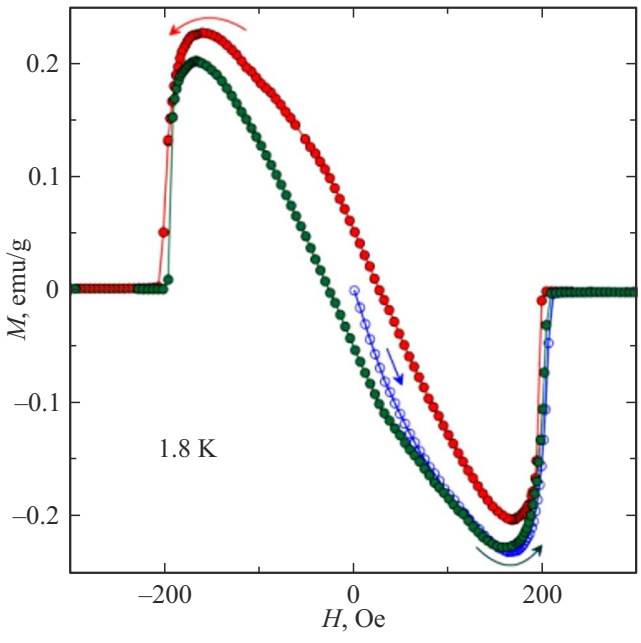

Figure 4. The magnetization isotherm obtained at 1.8 K in a porous glass/Ni/In nanocomposite.

can be seen from the shape of isotherm loop in Figure 1, freezing of the magnetic flux is the most likely cause of temperature hysteresis in the sample we studied.

4. Conclusion

The phase diagram $H(T)$ and the magnetization isotherms $M(H)$ for the superconducting nanocomposite porous glass/In−Ag alloy show that fractions of strongly and weakly bound indium segregates are formed in the nanocomposite. Strongly coupled segregates exhibit type-I superconductivity with a critical field and transition temperature close to the corresponding characteristics of bulk indium. In the system of weakly coupled indium segregates, there is type-II superconductivity which is characterized by a large critical field and strong pinning. The temperature of the superconducting transition in weakly bound indium segregates is increased due to the influence of size effects. The temperature hysteresis of the FCC and FCW magnetization is observed below the low-temperature transition and is presumably associated with the freezing of the magnetic flux in the intermediate state. The shift of branches of the magnetization isotherms is explained by the effects of the proximity of ferromagnetic and superconducting regions by analogy with the shift of the critical current maxima in heterostructures.

Acknowledgments

This study was supported by St. Petersburg State University, reg. No. EGISU NIOKTR: 125021702335-5. The measurements were performed using the equipment of the Resource Center of the „Centre for Diagnostics of Functional Materials for Medicine, Pharmacology and Nanoelectronics“ of the Saint Petersburg State University Research Park.

Conflict of interest

The authors declare that they have no conflict of interest.

References

[1] R. Wördenweber, V. Moshchalkov, S. Bending, F. Tafuri. Superconductors at the Nanoscale. From Basic Research to Applications. De Gruyter, Berlin (2017). 494 p.
[2] Y. Xiong, X. Lu. Metallic Nanostructures: From Controlled Synthesis to Applications. Springer International Publishing, Berlin (2015). 301 p.
[3] L.G. Sun, G. Wu, Q. Wang, J. Lu. Mater. Today **38**, 114 (2020).
[4] L. Ren, J. Zhuang, G. Casillas, H. Feng, Y. Liu, X. Xu, Y. Liu, J. Chen, I. Du, L. Jiang, S.X. Dou. Adv. Funct. Mater. **26**, 8111 (2016).
[5] S.-I. Shamoto, M.K. Lee, Y. Fujimura, K. Kondo, T.U. Ito, K. Ikeuchi, S. Yasuda, L.-J. Chang. Mater. Res. Express **8**, 076303 (2021).
[6] J.W. Ekin. Superconductor to Normal−Metal Contacts. In Handbook of Superconductivity. CRC Press: Boca Raton, FL, USA (2022). P. 448.
[7] R.I. Made, C.L. Gan, L.L. Yan, A. Yu, S.W. Yoon, J.H. Lau, C. Lee. J. Electron. Mater. **38**, 365 (2009).
[8] P.J. Rossi, N. Zotov, E.J. Mittemeijer. J. Appl. Phys. **120**, 165308 (2016).
[9] C.G. Granqvist. Solid State Commun. **16**, 581 (1975).
[10] C.G. Granqvist, T. Claeson. Solid State Commun. **32**, 531 (1979).
[11] Y.S. Ciou, M.K. Lee, E.V. Charnaya, C. Tien, L.J. Chang, Y.A. Kumzerov, M.I. Samoylovich. Supercond. Sci. Technol. **26**, 055009 (2013).
[12] J.H.P. Watson. Phys. Rev. **148**, 223 (1966).
[13] D.M. Gokhfeld, S.I. Popkov, A.A. Bykov. Phys. C **566**, 1353526 (2019).
[14] M.V. Likholetova, E.V. Charnaya, E.V. Shevchenko, Y.A. Kumzerov, A.V. Fokin. Nanomaterials **14**, 1792 (2024).
[15] Dvukhfaznye stekla: struktura, svojstva, primenenie / Otv. red. B.G. Varshal. Nauka, Leningrad (1991). 276 p. (in Russian).
[16] H. Okamoto, T.B. Massalski. Binary Alloy Phase Diagrams, 2nd ed. H. Okamoto, M.E. Schlesinger, E.M. Mueller, Eds. ASM International: Materials Park, OH, USA (1990).
[17] Z. Moser, W. Gasior, J. Pstrus, W. Zakulski, I. Ohnuma, X.J. Liu, Y. Inohana, K. Ishida. J. Electron. Mater. **30**, 1120 (2001).
[18] A. Kroupa, A.T. Dinsdale, A. Watson, J. Vrestal, J. Vízdal, A. Zemanova. JOM **59**, 20 (2007).
[19] J.F. Zhang, P.J. Guo, M. Gao, K. Liu, Z.Y. Lu. Phys. Rev. B **99**, 045110 (2019).
[20] B.G. Lazarev, E.E. Semenenko, A.I. Sudovtsov, V.M. Kuz'menko. Soviet Phys.−Doklady **10**, 1204 (1966).
[21] M.J. Graf, T.E. Huber, C.A. Huber. Phys. Rev. B **45**, 3133 (1992).
[22] C. Tien, C.S. Wur, K.J. Lin, E.V. Charnaya, Y.A. Kumzerov. Phys. Rev. B **61**, 14833 (2000).
[23] M. Tinkham. Introduction to Superconductivity. 2nd ed. Dover Publications (2004). 454 p.
[24] R.W. Shaw, D.E. Mapother, D.C. Hopkins. Phys. Rev. **120**, 88 (1960).
[25] M.V. Likholetova, E.V. Charnaya, E.V. Shevchenko, M.K. Lee, L.-J. Chang, Yu.A. Kumzerov, A.V. Fokin. Nanomater. **13**, 280 (2023).
[26] E.V. Charnaya, C. Tien, K.J. Lin, C.S. Wur, Y.A. Kumzerov. Phys. Rev. B **58**, 467 (1998).
[27] E.V. Shevchenko, E.V. Charnaya, M.K. Lee, L.-J. Chang, M.V. Likholetova, I.E. Lezova, Y.A. Kumzerov, A.V. Fokin. Physica C **574**, 1353666 (2020).
[28] S. Theodorakis, Z. Těsanović. Phys. Rev. B **40**, *10*, 6659 (1989).
[29] J. Provost, E. Paumier, A. Fortini. J. Phys. F Met. Phys. **4**, 439 (1974).
[30] R. Satariano, L. Parlato, A. Vettoliere, R. Caruso, H.G. Ahmad, A. Miano, L. Di Palma, D. Salvoni, D. Montemurro, L. Parlato, G.P. Pepe, F. Tafuri, G. Ausanio, D. Massarotti. Phys. Rev. B **103**, 224521 (2021).

[31] O.M. Kapran, T. Golod, A. Iovan, A.S. Sidorenko, A.A. Golubov, V.M. Krasnov. Phys. Rev. B **103**, 094509 (2021).
[32] L. Parlato, R. Caruso, A. Vettoliere, R. Satariano, H.G. Ahmad, A. Miano, D. Montemurro, D. Salvoni, G. Ausanio, F. Tafuri, G.P. Pepe, D. Massarotti, C. Granata, J. Appl. Phys. **127**, 193901 (2020).
[33] A.I. Buzdin. Rev. Mod. Phys. **77**, 935 (2005).
[34] R. Fermin, D. Van Dinter, M. Hubert, B. Woltjes, M. Silaev, J. Aarts, K. Lahabi. Nano Lett. **22**, 2209 (2022).
[35] Y. Sakamoto, Y. Oba, H. Maki, M. Suda, Y. Einaga, T. Sato, M. Mizumaki, N. Kawamura, M. Suzuki. Phys. Rev. B **83**, 104420 (2011).
[36] W.H. Li, C.W. Wang, C.Y. Li, C.K. Hsu, C.C. Yang, C.M. Wu. Phys. Rev. B **77**, 094508 (2008).
[37] J.R. Clem, Z. Hao. Phys. Rev. B **48**, 13774 (1993).

Translated by T.Zorina